American Mineralogist, Volume 95, pages 959–967, 2010

Bitikleite-(SnAl) and bitikleite-(ZrFe): New garnets from xenoliths of the Upper Chegem volcanic structure, Kabardino-Balkaria, Northern Caucasus, Russia

Irina O. Galuskina,[1,*] Evgeny V. Galuskin,[1] Thomas Armbruster,[2] Biljana Lazic,[2] Piotr Dzierżanowski,[3] Viktor M. Gazeev,[4] Krystian Prusik,[5] Nikolai N. Pertsev,[4] Antoni Winiarski,[6] Aleksandr E. Zadov,[7] Roman Wrzalik,[6] and Anatoly G. Gurbanov[4]

[1]Faculty of Earth Sciences, Department of Geochemistry, Mineralogy and Petrography, University of Silesia, Będzińska 60, 41-200 Sosnowiec, Poland
[2]Mineralogical Crystallography, Institute of Geological Sciences, University of Bern, Freiestrasse 3, CH-3012 Bern, Switzerland
[3]Institute of Geochemistry, Mineralogy and Petrology, University of Warsaw, al. Żwirki i Wigury 93, 02-089 Warszawa, Poland
[4]Institute of Geology of Ore Deposits, Petrography, Mineralogy and Geochemistry (IGEM), Russian Academy of Sciences, Staromonetny 35, 119017 Moscow, Russia
[5]Institute of Materials Science, University of Silesia, Bankowa 12, 40-007 Katowice, Poland
[6]August Chełkowski Institute of Physics, University of Silesia, Uniwersytecka 4, 40-007 Katowice, Poland
[7]OOO Science-Research Center NEOCHEM, Dmitrovskoye Highway 100/2, 127238 Moscow, Russia

Abstract

Two new antimonian garnets—bitikleite-(SnAl) $Ca_3SbSnAl_3O_{12}$ and bitikleite-(ZrFe) $Ca_3SbZrFe_3O_{12}$—have been found as accessory minerals in the cuspidine zone of high-temperature skarns in a carbonate-silicate xenolith at the contact with ignimbrites within the Upper Chegem structure in the Northern Caucasus, Kabardino-Balkaria, Russia. The bitikleite series forms a solid solution with garnets of the kimzeyite-schorlomite and toturite type. Antimony-garnets form crystals up to 50 μm across containing kimzeyite cores and thin subsequent zones of complex lakargiite-tazheranite-kimzeyite pseudomorphs after zircon. Bitikleite-(SnAl) has a = 12.5240(2) Å, V = 1964.40(3) Å^3 and bitikleite-(ZrFe) has a = 12.49 Å, V = 1948.4 Å^3 ($Ia\bar{3}d$, Z = 8). The strongest powder diffraction lines of bitikleite-(SnAl) are [d, Å (*hkl*)]: 4.407 (220), 3.118 (440), 2.789 (420), 2.546 (422), 1.973 (620), 1.732 (640), 1.668 (642), and 1.396 (840). The strongest calculated powder diffraction lines of bitikleite-(ZrFe) are [d, Å (*hkl*)]: 4.416 (220), 3.123 (440), 2.793 (420), 2.550 (422), 1.975 (620), 1.732 (640), 1.669 (642), and 1.396 (840). The Raman spectra of bitikleite garnets are similar to the spectra of kimzeyite and toturite. Larnite, rondorfite, wadalite, magnesioferrite, tazheranite, lakargiite, kimzeyite, and toturite associated with bitikleite garnets are typical of high-temperature (>800 °C) formation.

Keywords: Bitikleite-(SnAl), bitikleite-(ZrFe), new garnet, antimony, solid solution, single-crystal diffraction, Raman spectroscopy, Caucasus

Introduction

Natural garnets with significant antimony concentrations have only been recognized recently. Only toturite $Ca_3Sn_2Fe_2^{3+}SiO_{12}$ contains notable contents of Sb_2O_5 (up to 9 wt%) as was recently discovered in skarned xenoliths within ignimbrites of the Upper Chegem volcanic structure, Northern Caucasus, Kabardino-Balkaria, Russia (Galuskina et al. 2010b). Antimony in toturite substitutes at the octahedral site for one of two cations in accordance with the substitution scheme: $^{VI}Sn^{4+}\ ^{IV}Si \rightarrow\ ^{VI}Sb^{5+}\ ^{IV}Fe^{3+}$. This type of substitution suggested the possible existence of Sb-dominant natural garnets with a composition approaching $Ca_3(Sb^{5+}R^{4+})R_3^{3+}O_{12}$, where R^{4+} = Sn, Zr, Ti and R^{3+} = Fe, Al. Subsequently, a large number of garnets represented by the solid solution $Ca_3(Sn,Zr,Ti^{4+},Sb^{5+},U^{6+}...)_2(Fe^{3+},Al,Si,Ti^{4+}...)_3O_{12}$ were recognized in xenoliths located close to the top of a small ridge between the mountain peaks of Lakargi and Vorlan (coordinates 43°17′N 43°6.42′E). This approach finally led to the discovery of two antimonian garnets: bitikleite-(SnAl) $Ca_3SbSnAl_3O_{12}$ (IMA2009-052) and bitikleite-(ZrFe) $Ca_3SbZrFe_3^{3+}O_{12}$ (IMA2009-053), and also an uranian garnet elbrusite-(Zr) $Ca_3U^{6+}ZrFe_2^{3+}Fe^{2+}O_{12}$ (IMA2009-051, Galuskina et al. 2010a). All garnets cited above were approved by the CNMNC IMA in October 2009.

Altered xenoliths in ignimbrites near Lakargi Mt. are the source rocks of several recently discovered new minerals: calcio-olivine γ-Ca_2SiO_4 (Zadov et al. 2008), lakargiite $CaZrO_3$ (Galuskin et al. 2008), chegemite $Ca_7(SiO_4)_3(OH)_2$ (Galuskin et al. 2009), kumyubeite $Ca_5(SiO_4)_2F_2$ (Galuskina et al. 2009), $KNa_2Li(Mg,Fe)_2Ti_2Si_8O_{24}$ (IMA2009-009), and $CaUO_4$ (IMA2009-032). Bitikleite-(SnAl) was detected in xenolith 1, and bitikleite-(ZrFe) was found in xenolith 7, located 1.5 km to the west of xenolith 1 (see geological scheme in Galuskin et al. 2009). The Fe^{3+}-analog of kimzeyite with the crystal-chemical

* E-mail: irina.galuskina@us.edu.pl

formula of end-member $Ca_3Zr_2(Fe_2^{3+}Si)O_{12}$ is the most widespread garnet in altered xenoliths near Lakargi Mt. It forms a solid solution with garnets of the bitikleite series and with toturite. The Fe^{3+}-analog of kimzeyite from Kerimasi volcano, Tanzania, was recently approved by CNMCN IMA as a new mineral (IMA2009-029). It is to be noted that the Fe^{3+}-analog of kimzeyite and its structure has been previously studied (Schingaro et al. 2001; Galuskina et al. 2005; Whittle et al. 2007).

The dominant valence rule, considering a coupled heterovalent-homovalent substitution at the octahedral (Y) and tetrahedral (Z) sites and valency-imposed double site occupancy at the Y site (Hatert and Burke 2008) were used for determination of the end-member formulae of the bitikleite series. In addition, the bitikleite series forms a solid solution with Sn-Zr-garnets of the kimzeyite type. We use double Levinson-type suffices naming antimony garnets (Levinson 1966). The first suffix indicates the dominant cation at ½ of the two Y sites. The second suffix characterizes the dominant cation at the Z site. Thus, bitikleite-(SnAl) has the end-member formula $Ca_3SbSnAl_3O_{12}$ and bitikleite-(ZrFe) has the end-member formula $Ca_3SbZrFe_3^{3+}O_{12}$. As end-members of the bitikleite series are aluminates and ferrites, they should formally be classified as oxides. However, natural garnets of the bitikleite series form a solid solution with silicate garnets: toturite, kimzeyite, schorlomite. Thus, they are attributed to the garnet group. This case has a corresponding precedent with the hibschite-katoite series (hydrogrossular series), which is attributed to the garnet group, although katoite with the ideal end-member formula $Ca_3Al_2(H_4O_4)_3$ is a Si-free garnet (Mandarino and Back 2004).

The synthetic analog of bitikleite-(ZrFe) $Ca_3SbZrFe_3O_{12}$ (a = 12.669 Å) was synthesized more than 35 years ago (Dodokin et al. 1972). In addition, a garnet of $Ca_3SbSnFe_3O_{12}$ composition (a =12.634 Å) as an Fe^{3+}-analog of bitikleite-(SnAl) has been described by the same authors (Dodokin et al. 1972).

The name bitikleite is given after the geographical name Bitikle, which is the name of an old fortification, situated close to those skarned xenoliths where the new minerals were discovered. The fortification of Bitikle is a historical and cultural monument of the Russian nation. Holotype samples of bitikleite-(ZrFe) No. 3841/1 and bitikleite-(SnAl) No. 3842/1 are deposited in the collection of the Fersman Mineralogical Museum RAN, Moscow. In this paper, we present the results of investigations on new antimonian garnets and describe the associated minerals and their genesis.

Analytical methods

The morphology and composition of Sb-garnet crystals were investigated using a Philips/FEI ESEM XL30/EDAX scanning electron microscope and a CAMECA SX100 electron-microprobe analyzer. Electron microprobe analyses (EPMA) of garnets were performed at 15 kV and 40–50 nA using the following lines and standards: Mg$K\alpha$ = diopside; Al$K\alpha$ = orthoclase; Si$K\alpha$, Ca$K\alpha$ = wollastonite; Sc$K\alpha$ = Sc; Ti$K\alpha$ = rutile; V$K\alpha$ = V_2O_5; Cr$K\alpha$ = Cr_2O_3; Mn$K\alpha$ = rhodonite; Fe$K\alpha$ = hematite; Sr$L\alpha$ = $SrTiO_3$; Y$L\alpha$ = YAG; Zr$L\alpha$ = zircon; Nb$L\alpha$ = Nb; Sn$L\alpha$ = cassiterite; Sb$L\alpha$ = GaSb; Hf$M\alpha$ = Hf; Th$M\alpha$ = ThO_2; U$M\beta$ = UO_2.

The small size of bitikleite-(ZrFe) crystals necessitated the use of single-crystal electron backscatter diffraction (EBSD) analysis for the determination of structural parameters and symmetry. EBSD images were recorded with help of a HKL Nordlys II camera attached to the high-performance scanning electron microscope JSM-6480 using a beam energy of 30 kV. The microprobe thin section, on which composition measurements were performed, was re-polished using Al_2O_3 suspension of 20 nm particle size. Calibration of SEM and EBSD geometry was carried out with a Si single crystal for two detector distances: 177 mm (normal working position) and 150 mm (camera retracted position). The program "Chanel5" (Oxford Instruments) was used for interpretation of the obtained EBSD diffraction patterns.

Single-crystal X-ray studies were carried out using a Bruker APEX II SMART diffractometer, Mo$K\alpha$ radiation, λ = 0.71073 Å, at 50 kV and 35 mA.

A powdered sample was examined with a Rigaku D/max RAPID II X-ray diffractometer with a rotating anode, Ag$K\alpha$ radiation operated at 60 kV and 200 mA, equipped with $K\alpha$ monochromator and curved imaging plate systems for 2D X-ray scattering. PowderCell for Windows version 2.4 (Kraus and Nolze 1996), based on the Rietveld method, was used to refine the garnet unit-cell dimensions, and to calculate the XRD patterns.

Raman spectra of single crystals of garnet were recorded using a LabRam HR800 spectrometer (Jobin-Yvone-Horiba) equipped with a monochromator (1800 line/mm grating) and a charge-coupled device (CCD) comprising a Peltier-cooled detector (1024 × 256) and an Olympus BX40 confocal microscope. The incident laser excitation was provided by a water-cooled argon laser source operating at 514.5 nm. The power at the exit of the 100× objective lens varied from 40 to 60 mW. The Raman spectra were recorded at 0° geometry, in the range of 50–4000 cm^{-1} Raman shift and with a spectral resolution of 2.5 cm^{-1}. The collection time was 10 s and 16 scans were accumulated. The monochromator was calibrated using the Raman scattering line of a silicon plate (520.7 cm^{-1}).

Occurrence and description of bitikleite-series garnets

Bitikleite-(SnAl)

Bitikleite-(SnAl) was discovered in a 20–30 cm thick cuspidine-fluorite zone in close vicinity to the eastern contact of xenolith number 1 with unaltered ignimbrite. Xenolith 1, of more than 20 m in cross section, is the largest among known xenoliths located between the Lakargi and Vorlan peaks. The following zonation from center to rim is observed in the xenolith: (1) marble; (2) spurrite; (3) Ca-humite (chegemite, kumtyubeite, reinhardbraunsite); and (4) cuspidine (after larnite) zones. The cuspidine zone is often formed near the contact of the ignimbrite (micro-breccia?), marked by hydrogarnet pseudomorphs after phenocrysts of the original ignimbrite with many dispersed perovskite crystals. A full geological description of this area and of xenolith 1 is provided by Gazeev et al. (2006) and Galuskin et al. (2008, 2009). Bitikleite-(SnAl) is found in association with cuspidine, fluorite, wadalite, rondorfite, bultfonteinite, As-bearing fluor- and hydroxylellestadite (Pasero et al. 2010), ettringite group minerals, perovskite, magnesioferrite, F-bearing hibschite, afwillite, hillebrandite, and other undiagnosed Ca-hydrosilicates (Fig. 1a). Rare larnite relics were noted. Bitikleite-(SnAl) forms crystals {211} up to 50 μm, which are coated with a hibschite "jacket" (Fig. 1b). Usually, bitikleite-(SnAl) crystals contain Fe^{3+}-dominant kimzeyite cores (Fig. 1c; Table 1, analyses 1–3). Homogenous crystals are rather scarce (Fig. 1d; Table 1, analyses 4–6). In addition, bitikleite-(SnAl) frequently forms relatively homogenous zones on pseudomorphs of lakargiite after zircon (Fig. 1e; Table 1, analyses 7, 8). Bitikleite-(SnAl) is found in thin rims together with toturite and kimzeyite on porous lakargiite-tazheranite-kimzeyite pseudomorphs, probably formed after zircon (Fig. 1f, analyses 9–13).

Bitikleite-(SnAl) crystals are light yellow or colorless, with a white streak and strong vitreous luster. The new garnet is optically isotropic (n = 1.851, based on Gladstone-Dale calculation of analysis 14, Table 1). The calculated density for the composition of the holotype sample is 4.505 g/cm^3 (Table 1, analysis I).

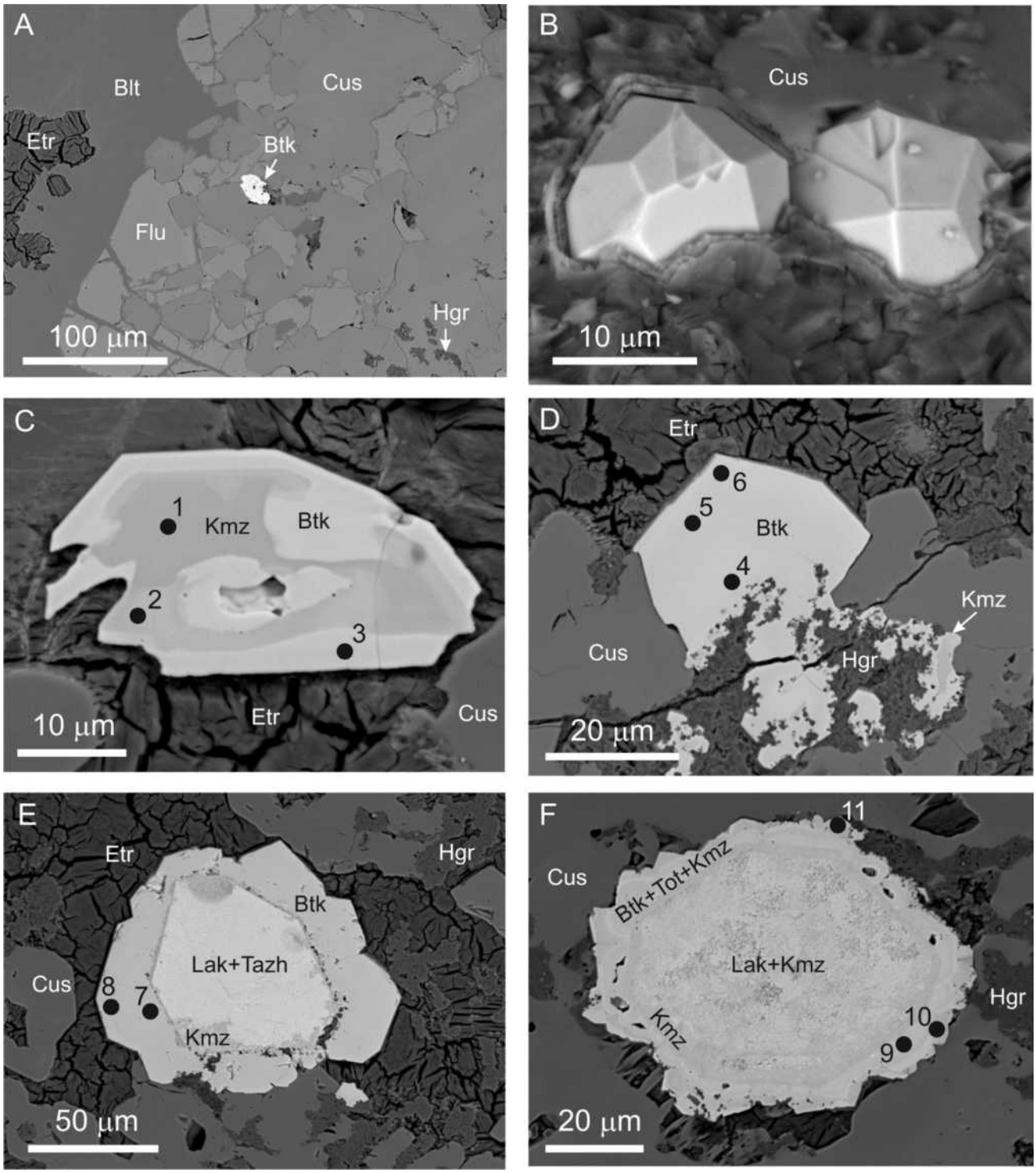

Figure 1. Occurrence and morphology of bitikleite-(SnAl): (**a**) crystal in cuspidine-fluorite skarn, (**b**) crystals confined by {211} forms, (**c**) zonal crystal composition, (**d**) homogeneous crystal, (**e**) bitikleite-(SnAl) rim on lakargiite-tazheranite pseudomorph, (**f**) bitikleite-(SnAl)-toturite-kimzeyite rim on complex pseudomorph. Blt = butfonteinite, Btk = bitikleite-(SnAl), Cus = cuspidine, Etr = ettringite group minerals, Fl = fluorite, Hgr = hibschite-katoite series, Kmz = kimzeyite, Lak = lakargiite, Tzh = tazheranite.

Bitikleite-(ZrFe)

Bitikleite-(ZrFe) was discovered in a thin cuspidine-hibschite zone of xenolith 7 in contact with unaltered ignimbrite (Fig. 2). Xenolith 7 was discovered in 2008; it is located 1.5 km from xenolith 1 and lacks a well-developed skarn zonation. It has a central chegemite zone with larnite relics, where the new mineral $(CaU^{6+})O_4$—an analog of uraninite—was detected, followed by an external cuspidine zone in contact with the ignimbrite (Galuskin et al. 2009). Bitikleite-(ZrFe) was found in the same mineral association as bitikleite-(SnAl). It occurs together with

TABLE 1. Chemical composition of bitikleite-(SnAl) and associated garnets

	I			II			III			1	2	3	4	5	6
	Mean 19	s.d.	Range	Mean 8	s.d.	Range	Mean 11	s.d.	Range	Kmz	Kmz	Btk	Btk	Btk	Btk
UO_3 wt%	0.05	0.06	0–0.17	0.02	0.04	0–0.12	n.d.			2.68	2.14	n.d.	0.12	n.d.	n.d.
V_2O_5	0.02	0.03	0–0.09	0.04	0.03	0–0.09	n.d.			n.d.	n.d.	n.d.	n.d.	n.d.	0.09
Nb_2O_5	0.07	0.06	0–0.22	0.08	0.06	0–0.19	0.04	0.05	0–0.15	0.30	0.17	n.d.	0.06	0.10	0.04
Sb_2O_5	25.98	1.66	23.66–28.80	26.73	1.98	24.69–28.11	24.57	1.05	22.46–26.00	0.07	0.07	28.17	28.32	17.86	28.21
SiO_2	0.28	0.11	0.06–0.44	0.32	0.08	0.22–0.42	0.46	0.10	0.33–0.66	9.09	6.48	0.19	0.2	1.08	0.27
TiO_2	2.66	1.06	1.45–4.73	3.10	0.72	2.05–4.14	2.06	0.25	1.55–2.40	7.10	4.64	1.98	3.32	3.83	3.98
ZrO_2	0.28	0.38	0–1.39	0.45	0.48	0.05–1.37	0.03	0.04	0–0.10	23.80	22.85	0.10	0.10	0.26	0.12
SnO_2	16.65	2.41	11.41–19.87	15.03	1.70	12.23–17.72	19.27	0.92	17.83–20.71	3.79	13.78	15.58	12.90	25.09	12.23
HfO_2	0.01	0.02	0–0.07	0.03	0.02	0–0.06	n.d.			0.47	0.35	n.d.	n.d.	n.d.	n.d.
ThO_2	n.d.						n.d.			n.d.	0.21	n.d.	n.d.	n.d.	n.d.
Al_2O_3	11.65	0.60	10.97–12.96	11.30	0.43	10.73–11.92	12.96	0.33	12.37–13.42	3.24	3.81	11.45	11.54	11.08	11.42
Sc_2O_3	n.d.						n.d.			1.37	0.24	0.47	n.d.	n.d.	n.d.
Cr_2O_3	0.02	0.02	0–0.08	0.01	0.01	0–0.03	n.d.			n.d.	0.04	0.10	n.d.	0.04	n.d.
Fe_2O_3	14.38	0.58	13.61–15.49	14.97	0.45	15.40–16.57	12.74	0.84	11.12–13.85	19.35	18.24	13.95	15.10	14.42	15.24
FeO	1.11			0.98			1.35	0.69	0–2.35	0.20	n.d	1.30	0.70	n.d.	1.11
SrO	0.01	0.01	0.01–0.03				n.d.			n.d.	n.d.	n.d.	0.08	0.04	n.d.
MnO	0.03	0.03	0–0.07	0.01	0.02	0–0.04	0.02	0.03	0–0.07	0.05	n.d.	0.05	n.d.	n.d.	n.d.
CaO	25.38	0.35	24.80–25.94	25.67	0.38	25.17–26.26	24.94	0.43	24.18–25.54	27.45	25.80	25.17	25.78	25.64	25.84
MgO	0.22	0.20	0–0.60	0.36	0.17	0.14–0.60	0.08	0.07	0.02–0.22	0.05	n.d.	0.52	0.54	0.01	0.47
Y_2O_3	<0.10			<0.10			<0.10			0.06	0.08	n.d.	n.d.	n.d.	n.d.
Total	98.81			99.10			98.52			99.07	98.82	99.03	98.76	99.45	99.02
Ca*	3.029			3.042			2.981			3.027	3.011	3.006	3.048	3.043	3.034
Th							0.002				0.005				
Sr	0.001												0.005	0.003	
Mn^{2+}	0.003			0.001						0.004		0.005			
Y										0.003	0.005				
Mg							0.013								
Fe^{2+}							0.004								
X	3.033			3.043			3			3.034	3.021	3.011	3.053	3.046	3.034
Sb^{5+}	1.075			1.099			1.019			0.003	0.003	1.167	1.161	0.735	1.149
Sn^{4+}	0.740			0.663			0.857			0.156	0.598	0.693	0.568	1.108	0.534
Zr	0.015			0.024			0.002			1.195	1.214	0.005	0.005	0.014	0.006
Ti	0.094			0.103			0.120			0.395	0.070		0.118	0.088	0.191
U^{6+}	0.001									0.058	0.049		0.003		
V^{5+}	0.001			0.003											0.007
Nb^{5+}	0.004			0.004			0.002			0.014	0.008		0.003	0.005	0.002
Hf				0.001						0.014	0.011				
Sc										0.123	0.023	0.046			
Cr	0.002			0.001							0.003	0.009		0.004	
Mg	0.037			0.059						0.008		0.086	0.089	0.002	0.077
Y	1.969			1.957			2			1.966	1.979	2.006	1.947	1.956	1.966
Al	1.530			1.473			1.704			0.393	0.489	1.505	1.501	1.447	1.475
Fe^{3+}	1.206			1.246			1.070			1.499	1.424	1.170	1.254	1.202	1.257
Fe^{2+}	0.104			0.091			0.122			0.017	0.071	0.121	0.065		0.101
Ti^{4+}	0.129			0.155			0.053			0.155	0.310	0.166	0.158	0.231	0.137
Si	0.031			0.035			0.051			0.936	0.706	0.021	0.022	0.120	0.030
Z	3			3			3.000			3	3	2.983	3	3	3

Notes: I–III = bitikleite-(SnAl) holotype sample: I = individual zoned crystals with and without kimzeyite core, II = heteregenous small crystals, III = zones up to 50 μm across on lakargiite-tazheranite pseudomorphs after zircon, 1–11 = points of garnet analyses shown in Figure 1; 12,13 = garnets from a rare type of lakargiite-kimzeyite pseudomorph after zircon with toturite-bitikleite zonal rim; 14 = bitikleite-(SnAl) crystal from intergrowth with the crystal used for single-crystal diffraction study (mean of 4 analyses).
* Calculated on 12 O, Fe^{3+}/Fe^{2+} calculated on charge balance.

cuspidine, larnite, wadalite, rondorfite, fluorite, hydroxylellestadite, ettringite group minerals, perovskite, magnesioferrite, hibschite, afwillite, hillebrandite, tobermorite-like minerals, and hydrocalumite. The ubiquitous occurrence of hibschite in rocks with bitikleite-(ZrFe) (Fig. 2a) most probably indicates that wadalite-mayenite minerals were the main Al-bearing phases of the primary skarn. Bitikleite-(ZrFe) forms aggregates with lakargiite and Fe^{3+}-dominant kimzeyite (Figs. 2a and 2b; Table 2, analyses 1–3), replacing altered zircon. Porous xenomorphic grains usually represent bitikleite-(ZrFe) as well (Fig. 2c; Table 2, analysis 4). Crystals up to 10 μm in size are often confined by {110} forms in contrast to bitikleite-(SnAl) crystals for which {211} forms prevail (Figs. 1b and 2a). Bitikleite-(ZrFe) is light brown or yellow with strong vitreous luster; the streak is white with yellow tint. It is optically isotropic, n ≈ 1.9. The calculated density for the garnet composition of the holotype sample (Table 2, analysis I) is 4.470 g/cm^3.

STRUCTURAL DATA AND RAMAN SPECTROSCOPY

Initially, structural data were obtained using EBSD (Fig. 3) for garnet shown in Figure 1c (Table 1, analyses 1–3), in which three zones are distinguished: core = kimzeyite, intermediate zone = stannian kimzeyite, rim = bitikleite-(SnAl). EBSD patterns of these three garnets look almost identical and fitting of Kikuchi images led to very similar cell parameters at MAD (mean angular deviation) = 0.19–0.37° (representing excellent to very good fitting results).

Later, we were able to extract a 50 μm monocrystal of bitikleite-(SnAl). This crystal, intended to be studied by single-crystal X-ray methods, was first analyzed by SEM/EDS and

TABLE 1.—*EXTENDED*

7	8	9	10	11	12	13	14
Btk	Btk	Tot	Kmz	Btk	Tot	Btk	Btk
n.d.	n.d.	0.72	0.67	n.d.	2.23	n.d.	n.d.
0.03	n.d.	n.d.	0.06	n.d.	0.14	n.d.	0.06
0.07	n.d.	0.18	0.12	0.14	0.34	0.11	0.06
23.80	25.12	n.d.	0.04	12.86	0.03	25.74	24.71
0.48	0.44	4.71	6.63	2.13	4.78	0.31	0.43
1.98	1.55	5.01	3.77	4.61	5.30	1.96	2.26
0.10	0.08	9.06	23.66	0.36	12.70	0.1	0.68
20.42	19.61	32.41	14.63	30.23	26.88	18.24	18.71
n.d.	n.d.	0.29	0.42	n.d.	0.19	n.d.	0.03
n.d.	n.d.	0.29	0.15	n.d.	0.09	n.d.	n.d.
13.13	13.42	5.04	4.80	10.18	5.55	13.13	12.83
0.52	0.56	0.03	0.09	0.27	0.07	0.62	n.d.
n.d.	n.d.	0.03	0.05	n.d.	n.d.	n.d.	n.d.
11.11	11.96	15.72	16.84	13.76	14.33	12.74	12.85
2.36	1.72	n.d.	n.d.	n.d.	1.22	1.37	1.40
0.06	0.13	n.d.	n.d.	0.03	n.d.	n.d.	n.d.
n.d.	n.d.	0.04	n.d.	n.d.	n.d.	n.d.	n.d.
24.18	24.73	25.12	26.32	25.88	24.85	25.2	25.29
0.02	0.08	n.d.	n.d.	0.03	0.02	n.d.	0.10
n.d.	n.d.	n.d.	n.d.	n.d.	n.d.	0.16	n.d.
98.27	99.41	98.65	98.25	100.48	98.73	99.71	99.41
2.907	2.934	3.039	3.060	3.040	2.977	2.970	2.995
		0.007	0.004		0.002		
0.004	0.008			0.002			
		0.004					
0.003	0.014				0.003	0.027	0.005
0.086	0.044				0.018	0.003	
3	3	3.050	3.064	3.042	3	3	3
0.993	1.035		0.002	0.524	0.001	1.052	1.014
0.913	0.866	1.459	0.633	1.322	1.200	0.801	0.825
0.005	0.004	0.499	1.252	0.019	0.692	0.005	0.037
0.031	0.041		0.018	0.065	0.014	0.076	0.105
		0.017	0.015		0.052		
0.003			0.004		0.011		0.004
0.004		0.009	0.006	0.007	0.017	0.006	0.003
		0.009	0.013		0.006		0.001
0.051	0.054	0.003	0.009	0.026	0.007	0.059	
		0.003	0.004				
				0.005			0.12
2	2	1.999	1.956	1.968	2	2	3
1.736	1.751	0.671	0.614	1.316	0.731	1.702	1.671
0.938	0.997	1.336	1.376	1.136	1.206	1.055	1.069
0.136	0.115				0.096	0.123	0.129
0.136	0.088	0.425	0.290	0.315	0.432	0.086	0.083
0.054	0.049	0.532	0.720	0.233	0.535	0.034	0.048
3	3	2.964	3	3	3	3	3

subsequently by electron microprobe (EMPA) (Table 1, analysis 14). Single-crystal structure refinement of bitikleite-(SnAl) with $a = 12.5240(2)$ Å, $V = 1964.40(3)$ Å^3 (Tables 3–5) shows that its structure is close to that of the synthetic garnet $YCa_2SbFe_4O_{12}$ with $a = 12.521(1)$ Å (Berry et al. 1995). In the structure refinement of bitikleite-(SnAl), the octahedral occupancy was modeled by Sb and Ti, yielding a reduced number of electrons (ca. 42 e^-; Table 4) in comparison with the value (ca. 49 e^-) obtained by EMPA data (Table 1, analysis 14). On the other hand, site occupancy refinement of the tetrahedral site led to 19 e^-, whereas analytical data (Table 1, analysis 14) yielded ca. 18.5 e^-. The dominance of transition-metal ions (mainly Fe) in tetrahedral coordination is also indicated by the unusual long T-O distance of 1.807(3) Å. Although the garnet crystal used for the single-crystal investigation had an EDS spectrum typical of bitikleite-(SnAl), this crystal probably had a kimzeyite core (Zr,Ti-rich), characteristic of garnets from xenolith 1 (Fig. 1c). This in turn decreases the number of electrons measured on the octahedral site. The kimzeyite core may also contribute to the increase of

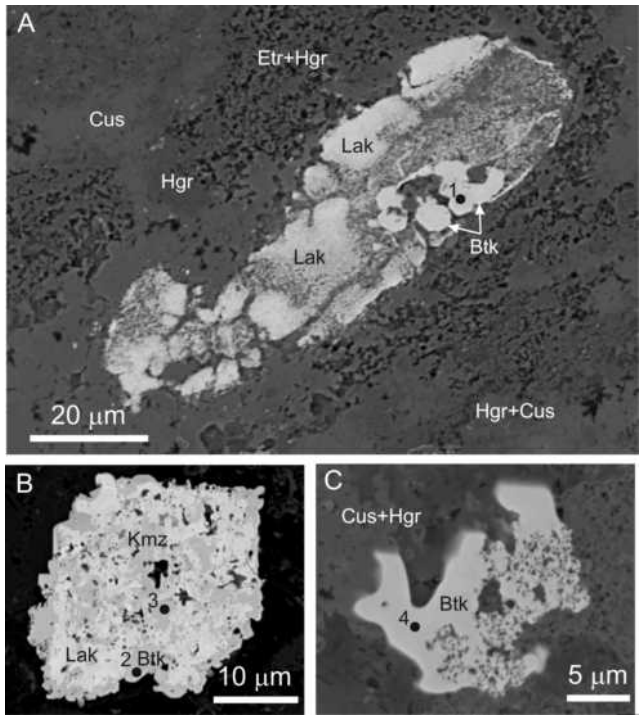

FIGURE 2. Occurrence and morphology of bitikleite-(ZrFe): (**a**) {110} crystals within a lakargiite aggregate in the cuspidine-hydrogarnet zone, (**b**) bitikleite-(ZrFe) as part of a complex pseudomorph, (**c**) xenomorphic porous crystal. Btk = bitikleite-(ZrFe), other symbols as in Figure 1.

the cell parameter {$^{VI}Sn^{4+}$ 50 (electrons)/0.69Å [ionic radius (Shannon 1976)] and $^{VI}Sb^{5+}$ 51/0.60 Å → ^{VI}Zr 40/0.72 Å and ^{IV}Al 13/0.39 Å → $^{IV}Fe^{3+}$ 26/0.49 Å}. In addition, μXRD powder diffraction data (Table 6) were collected for an aggregate of crystals (60 × 75 μm in size) of bitikleite-(SnAl). These data provided $a = 12.492(1)$ Å and $V = 1949.38(3)$ Å^3, which is significantly lower than the value refined from single-crystal data, probably indicating higher Sb^{5+} concentrations.

Structural data of bitikleite-(ZrFe) were obtained for a homogenous fragment of a porous xenomorphic grain (Fig. 2c; Table 2, analysis 4) using an EBSD detector (Fig. 4). Interpretation of EBSD data and subsequent structural modeling is based on the previously refined structure of bitikleite-(SnAl). The modeled bitikleite-(ZrFe) Kikuchi pattern showed a very good fit to the garnet type structure with MAD = 0.40° at a = 12.49(3) Å. Calculated powder diffraction data were obtained using EBSD data of bitikleite-(ZrFe) (Table 6).

Raman spectra of bitikleite-(SnAl) and bitikleite-(ZrFe) resemble spectra of silicate garnets with Zr and Sn, kimzeyite and toturite, the main bands of which are related to vibrations of (ZO_4) tetrahedra (Fig. 5; Schingaro et al. 2001; Galuskina et al. 2005, 2010b). In the Raman spectrum of kimzeyite, forming a core in the bitikleite-(SnAl) crystal (Fig. 5, spectrum 1), a strong band at 810 cm^{-1} and weak bands near 930 and 880 cm^{-1}, interpreted as Si-O stretching vibrations of $(SiO_4)^{4-}$ tetrahedra, are observed. These bands are significantly weaker in bitikleite spectra (Fig. 5, spectra 2–4). In the bitikleite spectra, the bands with maxima at ca. 790–800 cm^{-1}, related to symmetric Al-O stretching vibra-

TABLE 2. Composition of bitikleite-(ZrFe) and Fe^{3+}-dominant kimzeyite from xenolith 7

	I			1	2	3	4
	Mean 11	s.d.	Range	Btk	Btk	Kim	Btk
UO_3 wt%	0.64	0.51	0.16–1.96	0.16	0.71	0.89	1.96
V_2O_5	0.03	0.03	0–0.08	0.06	n.d.	n.d.	0.07
Nb_2O_5	0.18	0.17	0.03–0.66	0.15	0.17	0.17	0.66
Sb_2O_5	18.79	1.75	15.62–21.95	21.64	18.78	8.17	19.19
SiO_2	1.52	0.33	0.92–1.97	0.99	1.44	3.17	1.73
TiO_2	2.39	0.39	1.90–3.09	2.09	2.30	5.92	2.10
ZrO_2	15.92	2.28	11.63–18.86	12.4	16.29	26.13	14.84
SnO_2	6.15	1.90	2.16–9.10	8.51	6.40	2.40	2.16
HfO_2	0.25	0.09	0.09–0.38	0.13	0.24	0.54	0.31
ThO_2	0.04	0.06	0–0.16	n.d.	0.13	n.d.	n.d.
Al_2O_3	8.29	0.53	7.26–9.07	8.36	8.13	6.34	7.26
Sc_2O_3	n.d.			n.d.	n.d.	0.02	0.05
Cr_2O_3	0.02	0.02	0–0.08	n.d.	n.d.	n.d.	0.08
Fe_2O_3	18.74	1.73	17.34–23.62	18.6	17.34	18.15	23.64
FeO	0.87	0.61	0-1.72	1.52	1.62	0.32	0.64
MgO	0.06	0.04	0–0.14	0.08	0.06	0.02	n.d.
CaO	25.54	0.43	24.89–26.40	25.24	25.08	26.10	25.33
Total	99.43			99.93	98.69	98.33	100.02
Ca*	3.002			2.984	2.989	3.016	2.954
Th	0.001				0.003		
Mg				0.013	0.008		
Fe^{2+}				0.003			0.046
X	3.003			3	3	3.016	3
Sb^{5+}	0.766			0.888	0.776	0.327	0.776
Zr	0.852			0.668	0.884	1.374	0.788
Sn^{4+}	0.269			0.374	0.284	0.103	0.094
Ti^{4+}	0.067			0.051	0.020	0.130	0.172
U^{6+}	0.015			0.004	0.017	0.020	0.045
V^{5+}	0.002			0.004			0.005
Nb^{5+}	0.009			0.007	0.009	0.008	0.032
Hf	0.008			0.004	0.008	0.017	0.010
Sc						0.002	0.005
Cr	0.002						0.007
Mg	0.010				0.002	0.003	1.934
Fe^{3+}							0.053
Fe^{2+}							0.013
Y	2			2	2	1.984	2
Fe^{3+}	1.548			1.545	1.451	1.473	1.883
Al	1.072			1.087	1.066	0.806	0.931
Si	0.167			0.109	0.160	0.342	0.188
Ti^{4+}	0.130			0.122	0.172	0.350	
Fe^{2+}	0.080			0.137	0.151	0.029	
Z	2.997			3	3	3	3

Notes: I = xenomorphic grain from holotype sample; 1–4 = points of analyses in Figure 3.
*Calculated on 12 O, Fe^{3+}/Fe^{2+} calculated on charge balance.

TABLE 3. Data collection and structure refinement parameters for bitikleite-(SnAl)

Diffractometer	APEX II SMART
X-ray radiation	MoKα λ = 0.71073 Å
X-ray power	50 kV, 35 mA
Monochromator	graphite
Temperature	296(2) K
Theta range for data collection	3.99 to 30.5°
Index ranges	$-17 \le h \le 17, -17 \le k \le 17, -17 \le l \le 15$
Reflections collected	7637
Independent reflections	255 [$R_{(int)}$ = 0.0477]
Crystal size	0.02 × 0.04 × 0.05 mm³
Crystal system	cubic
Space group	$Ia\bar{3}d$
Unit-cell dimension	a = 12.5240(2) Å
Volume	1964.40(5) Å³
Z	8
Goodness-of-fit on F^2	1.272
Number of least-square param.	19
Final R value, $I > 2\sigma(I)$	159 reflections, $R1$ = 0.0211
Final R values, all data	$R1$ = 0.0401, wR_2 = 0.0582

TABLE 4. Atomic coordinates, equivalent isotropic atomic displacement parameters (Å²), site-occupation factors (*sof*, e^-), and bond lengths (Å) for bitikleite-(SnAl)

Site	Atom	x	y	z	U_{eq}	*sof*	e^-
X	Ca1	0.125	0	0.25	0.0116(4)	1.0	20
Y	Sb2	0	0	0	0.00699(19)	0.681(8)	41.75
	Ti2				0.00699(19)	0.319(8)	
Z	Fe3	0.375	0	0.25	0.0073(5)	0.462(12)	19
	Al3				0.0073(5)	0.538(12)	
O	O1	0.0323(2)	0.0503(2)	0.6516(2)	0.0144(6)	1.0	8
	X-O = 2.408(3) × 4			*Y*-O = 2.040(3) × 6			
	X-O = 2.555(3) × 4			*Z*-O = 1.807(3) × 4			

TABLE 5. Anisotropic mean-square displacement parameters (Å²) for bitikleite-(SnAl)

Site	U_{11}	U_{22}	U_{33}	U_{23}	U_{13}	U_{12}
X	0.0096(8)	0.0126(5)	0.0126(5)	0.0026(6)	0	0
Y	0.0069(2)	0.0069(2)	0.0069(2)	0.00000(17)	0.00000(17)	0.00000(17)
Z	0.0053(8)	0.0083(5)	0.0083(5)	0	0	0
O	0.0144(13)	0.0149(15)	0.0139(14)	–0.0004(11)	0.0017(11)	–0.0009(10)

TABLE 6. XRD powder patterns of bitikleite garnets

	bitikleite-(SnAl)[1]				bitikleite-(ZrFe)[2]	
hkl	d (Å)$_{obs}$	I_{obs}	d (Å)$_{cal}$	I_{cal}	d (Å)$_{cal}$	I_{cal}
211	5.1295	1	5.0998	1	5.0990	1
220	4.4068	77	4.4165	71	4.4159	60
400	3.1185	93	3.1230	87	3.1225	71
420	2.7889	62	2.7933	56	2.7929	55
332	2.6633	5	2.6633	6	2.6629	7
422	2.5460	97	2.5499	77	2.5495	97
431	2.4451	6	2.4498	7	2.4495	5
521	2.2784	3	2.2807	3	2.2804	3
440	2.2053	3	2.2083	3	2.2080	6
611	2.0248	3	2.0264	3	2.0262	4
620	1.9729	20	1.9751	19	1.9749	21
640	1.7316	15	1.7323	15	1.7321	22
642	1.6685	100	1.6693	100	1.6691	100
800	1.5613	9	1.5615	9	1.5613	18
822	1.4713	8	1.4722	8	1.4720	11
840	1.3960	15	1.3966	14	1.3964	26
842	1.3632	5	1.3630	5	1.3628	12
664	1.3316	13	1.3316	13	1.3314	21
844	1.2756	4	1.2749	4	1.2748	6
10.2.0	1.2255	5	1.2249	5	1.2248	7
10.4.0	1.1597	4	1.1598	4	1.1597	13
10.4.2	1.1397	9	1.1403	9	1.1402	40
880	1.1042	9	1.1041	9	1.1040	16
10.6.0	1.0722	1	1.0712	1	1.0710	2
12.0.0	1.0409	4	1.0410	4	1.0408	3
12.2.2	1.0131	14	1.0132	14	1.0131	19

Notes: 1 = Rigaku Rapid II, AgKα, 2 = calculated for CoKα and Debye-Scherrer geometry.

tions of $(AlO_4)^{5-}$, and at ca. 730–750 cm^{-1}, related to symmetric Fe-O stretching vibrations of $(Fe^{3+}O_4)^{5-}$ tetrahedra, are noted. The image is complicated by symmetric Ti-O stretching vibrations of $(TiO_4)^{4-}$ tetrahedra broadening the bands between 800 and 700 cm^{-1}. A band near 600 cm^{-1} is clearly visible in the bitikleite spectra. This band is most probably caused by asymmetric stretching vibrations in $(Fe^{3+}O_4)^{3-}$ tetrahedra (Rulmont et al. 1995).

Strong bands on the bitikleite spectra near 500 cm^{-1} [$(Z\text{-}O)_{bend.}$] and 300 cm^{-1} [$R(ZO_4)$] are significantly shifted toward lower frequencies in comparison to silicate garnets (Kolesov and Geiger 1998). Bands below 300 cm^{-1} represent translational motions of $T(ZO_4)$ and $T(Ca^{2+})$.

Differences in bitikleite-(SnAl) and bitikleite-(ZrFe) spectra are especially obvious in the 200–400 cm^{-1} region (Fig. 5). A band with a maximum near 300 cm^{-1} is characteristic of bitikleite-

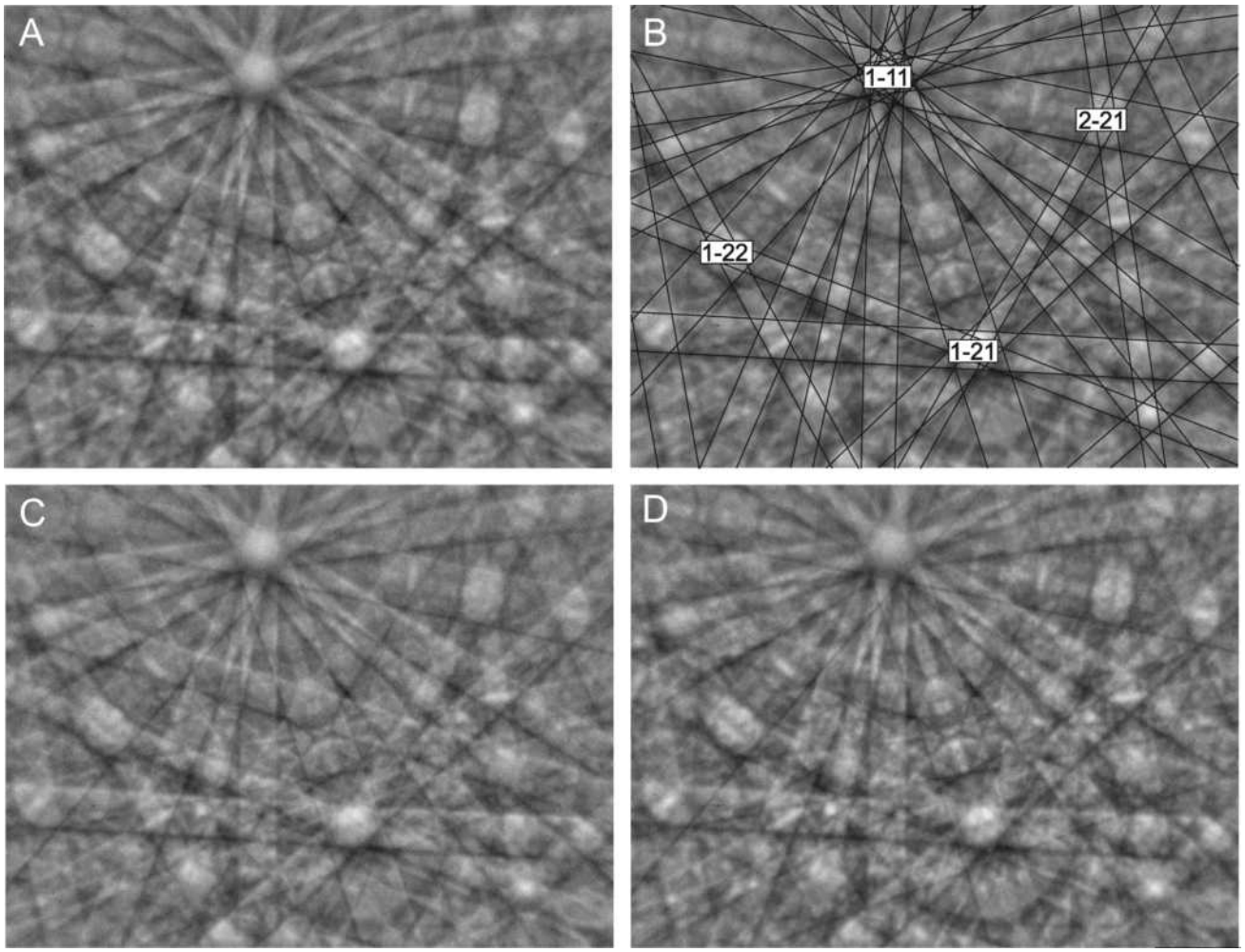

FIGURE 3. EBSD patterns obtained for separate zones of the crystal shown in Figure 1c: (**a**, **b**) bitikleite-(SnAl) rim, MAD = 0.37, *a* = 12.49 Å; (**c**) kimzeyite core, MAD = 0.19, *a* = 12.42 Å; (**d**) stannian kimzeyite intermediate zone, MAD = 0.21, *a* = 12.49 Å.

(SnAl), but is also characteristic of toturite (Fig. 5, spectrum 5); i.e., for Sn-dominant garnets. In Zr-dominant garnets [bitikleite-(ZrFe) and Fe^{3+}-dominant kimzeyite], this band appears at a lower frequency, near 293 cm^{-1}. The band near 244 cm^{-1}, which also appears in the toturite spectrum, is characteristic of garnets with predominant Fe^{3+} at the tetrahedral Z site. In the bitikleite-(SnAl) spectra this band shifts toward higher frequency with a maximum near 252 cm^{-1}.

CLASSIFICATION OF ZR-SN-SB-BEARING CA-GARNETS FROM LAKARGI SKARNS: END-MEMBERS AND COMPOSITIONAL TRENDS

Calcium antimonian garnets from cuspidine-fluorite zones of skarns in altered xenoliths from ignimbrites near Lakargi Mt. are represented by solid solution $Ca_3(Sb^{5+},Zr,Sn^{4+},Ti,U^{6}\ldots)_2(Fe,Al,Si,Ti\ldots)_3O_{12}$. Distinction of end-members is very difficult because of wide compositional variations and different strategies as to how end-members may be defined (Tables 1 and 2). Following the recommendations of Hatert and Burke (2008), we constructed a triangular classification diagram for garnets from xenoliths 1 and 7 with kimzeyite-schorlomite $Ca_3(Zr,Ti)_2R^{3+}_2R^{4+}O_{12}$–bitikleite $Ca_3SbR^{4+}R^{3+}_3O_{12}$–toturite $Ca_3Sn_2R^{3+}_2R^{4+}O_{12}$ (Fig. 6) defining the corners. For comparison, points representing garnet analyses from xenolith 3, from which Sb-bearing toturite was found, were added. In addition, analyses of Fe^{3+}-dominant kimzeyite from xenolith 5 were also included in this diagram (Galuskina et al. 2010b). There are three main trends of solid solutions for these garnets between: (1) Fe^{3+}-dominant kimzeyite and toturite; (2) toturite and bitikleite-(SnAl); and (3) Fe^{3+}-dominant kimzeyite and bitikleite-(ZrFe) (Fig. 6). By varying cation occupations at the structural sites of the bitikleite series, the following main end-members are obtained: $Ca_3(Sb^{5+}Sn^{4+})Al_3O_{12}$ [bitikleite-(SnAl)], $Ca_3(Sb^{5+}Zr)Al_3O_{12}$ (not found as yet), $Ca_3(Sb^{5+}Sn^{4+})Fe^{3+}_3O_{12}$ (only synthetic phase, Dodokin et al. 1972), and $Ca_3(Sb^{5+}Zr)Fe_3O_{12}$ [bitikleite-(ZrFe)]. Relatively high Ti content in some analyses of bitikleite-(SnAl) (for example, Table 1, analysis 6) indicates other possible end-members, such as $Ca_3(Sb^{5+}Ti^{4+})Al_3O_{12}$ and $Ca_3(Sb^{5+}Ti^{4+})Fe^{3+}_3O_{12}$.

The crystal-chemical formulae of bitikleite-(SnAl) and bitikleite-(ZrFe) from the holotype samples are (Table 1, analysis 1; Table 2, analysis 1)

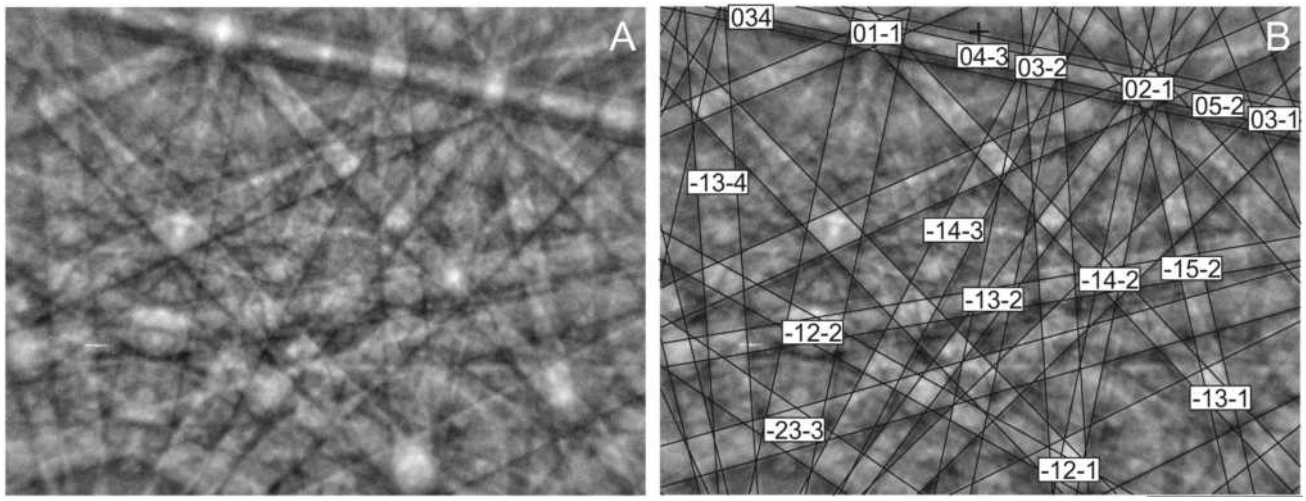

FIGURE 4. EBSD patterns (**a**) and indexing (**b**) obtained for crystal shown in Figure 2c, MAD = 0.40, a = 12.49 Å.

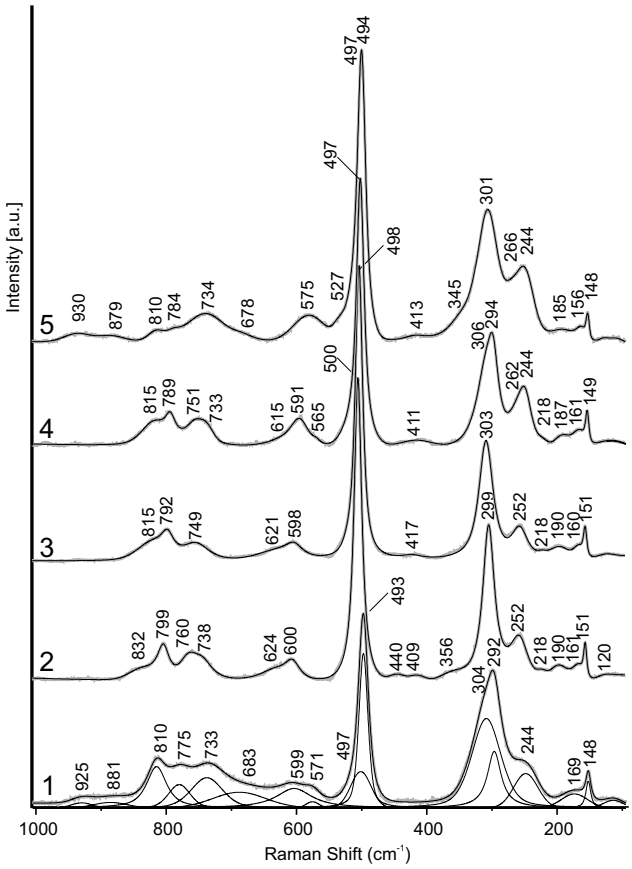

FIGURE 5. Raman spectra of garnets from Lakargi: 1, 2 = zonal crystal shown in Figure 1c: 1 = Fe^{3+}-dominant kimzeyite, 2 = bitikleite-(SnAl); 3 = bitikleite-(SnAl) in Figure 1d; 4 = bitikleite-(ZrFe) in Figure 2c; 5 = toturite (Galuskina et al. 2010b).

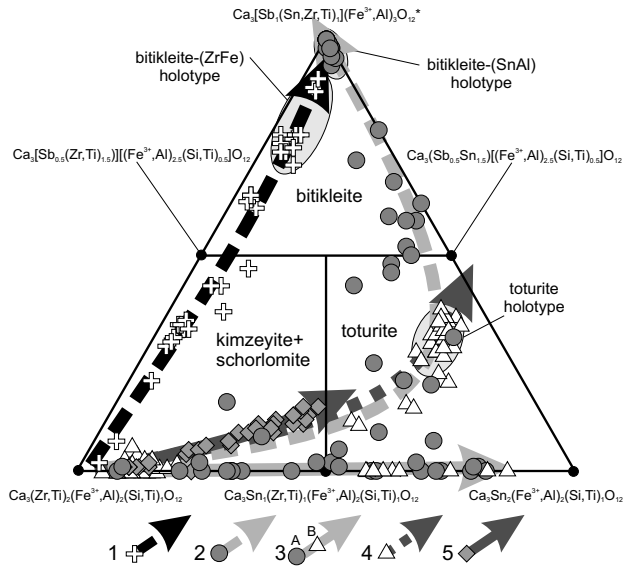

FIGURE 6. Analytical points of Lakargi garnets are shown in a triangular classification diagram. In addition, arrows indicate compositional trends: 1 = xenolith 7, 2 = xenolith 1, 3 = xenolith 1 (A) and xenolith 3 (B), 4 = xenolith 3, 5 = xenolith 5. The asterisk means including exotic Sb end-members (see text).

$(Ca_{3.029}Mn^{2+}_{0.003}Sr_{0.001})_{\Sigma 3.033}(Sb^{5+}_{1.075}Sn^{4+}_{0.740}Ti^{4+}_{0.095}Mg_{0.037}Zr_{0.015}Nb^{5+}_{0.004}Cr_{0.002}U^{6+}_{0.001})_{\Sigma 1.969}(Al_{1.530}Fe^{3+}_{1.206}Ti^{4+}_{0.128}Fe^{2+}_{0.104}Si_{0.031}V^{5+}_{0.001})_{\Sigma 3}O_{12}$ (1)

$(Ca_{3.002}Th_{0.001})_{\Sigma 3.003}(Sb^{5+}_{0.776}Zr_{0.852}Sn^{4+}_{0.269}Ti^{4+}_{0.067}Mg_{0.010}Nb^{5+}_{0.009}Hf_{0.008}Cr_{0.002}U^{6+}_{0.015})_{\Sigma 2}(Fe^{3+}_{1.548}Al_{1.072}Si_{0.167}Ti^{4+}_{0.130}Fe^{2+}_{0.080}V^{5+}_{0.002})_{\Sigma 2.997}O_{12}$. (2)

It is necessary to emphasize that we give only one among many possible variants of end-member definitions. The following end-members contribute to the composition of holotype bitikleite-(SnAl): $Ca_3Sb^{5+}Sn^{4+}Al_3O_{12}$ = 51% [bitikleite-(SnAl)], $Ca_3Sb^{5+}Sn^{4+}Fe^{3+}_3O_{12}$ = 23% ["bitikleite-(SnFe)"], $Ca_3Sb^{5+}Ti^{4+}Fe^{3+}_3O_{12}$ = 9% ["bitikleite-(TiFe)"], $Ca_3Sb^{5+}Zr^{4+}Fe^{3+}_3O_{12}$ = 1.5% [bitikleite-(ZrFe)]. The sum of bitikleite end-members is 84.5%, the other end-members are more exotic with the Y site fully occupied by Sb^{5+}: $Ca_3Sb^{5+}_2(Mg,Fe^{2+})Fe^{3+}_2O_{12}$ = 7%. This end-member may solve the problem of compositions with Sb > 1 apfu in some analyses of bitikleite-(SnAl) (Table 1), $Ca_3Sb^{5+}(Mg,Fe^{2+})Ti^{4+}_2Fe^{3+}O_{12}$ = 7%, $Ca_3Sb^{5+}(Mg,Fe^{2+})Si_2Fe^{3+}O_{12}$ = 1.5%.

End-members calculated for bitikleite-(ZrFe) are as follows: $Ca_3SbZrFe_3^{3+}O_{12}$ = 52% [bitikleite-(ZrFe)], $Ca_3SbZrAl_3O_{12}$ = 25% ["bitikleite-(ZrAl)"]. The sum of bitikleite end-members is 77%. The others are as follows: $Ca_3Sn_2TiAl_3O_{12}$ = 11% ["toturite-(TiAl)"], $Ca_3Sn^{4+}Fe^{2+}Si_3O_{12}$ = 5% ["morimotoite-(Sn)"], $Ca_3Zr_2TiAl_2O_{12}$ = 4% ["kimzeyite-(Ti)"], $Ca_3Ti_2SiAl_2O_{12}$ = 4% ["schorlomite-(Al)"].

The holotype sample of bitikleite-(SnAl) is less complex in composition than that of bitikleite-(ZrFe). Bitikleite-(SnAl) contains impurities of Ti and Fe (>1 wt%) (Table 1), and bitikleite-(ZrFe) displays significant impurities of Sn, Ti, Si, Al, and U (Table 2).

Zonation found in calcium garnets from skarns near Lakargi Mt. allows the tracing of common trends of compositional change shown in the classification diagram (Fig. 6). Zirconian garnets of kimzeyite type, which form separate crystals and are also part of complex pseudomorphs after zircon within the endocontact zone (contact breccia), crystallize first together with lakargiite $CaZrO_3$ and tazheranite (cubic ZrO_2) stabilized by Ca impurities. Zirconian garnets are modified to stannian garnets—toturite, subsequently succeeded by antimonian-stannian garnets of bitikleite-(SnAl) type. This sequence is characteristic of the compositional evolution in xenolith 1. An absence of Sn leads to crystallization of antimonian garnets of bitikleite-(ZrFe) type directly after kimzeyite. The appearance of thin subsequent zones of kimzeyite (Fig. 1f) is related to dissolution of early skarn minerals–zirconium oxides.

The formation of bitikleite garnets is due to high-temperature contact alteration of carbonate xenoliths within the diatreme facies of ignimbrites (age 2.8–3.0 Ma) in the larnite facies of contact metamorphism (temperatures of 800–1000 °C and low pressures) (Gazeev et al. 2006; Galuskin et al. 2008, 2009).

Acknowledgments

I.G. was financially supported by the Ministry of Science and Higher Education of Poland, grants N N307 097038. The research was also partly supported by the Russian Foundation of Basic Researches, Project 08-05-00181. The authors thank Jan Zalasiewicz (University of Leicester) for English correction.

References cited

Berry, F.J., Davalos, J., Greaves, C., Marco, J.F., Slaski, M., Slater, P.R., and Vithal, M. (1995) Magnetic ordering in the garnet YCa_2SbFeO_{12}. Journal of Solid State Chemistry, 115, 435–440.

Dodokin, A.P., Lyubutin, I.S., Mill', B.V., and Peshkov, V.P. (1972) Mössbaueer effect in antiferromagnetic substances with garnet structures. Journal of Experimental and Theoretical Physics, 63, 1002–1009 (in Russian).

Galuskin, E.V., Gazeev, V.M., Armbruster, T., Zadov, A.E., Galuskina, I.O., Pertsev, N.N., Dzierżanowski, P., Kadiyski, M., Gurbanov, A.G., Wrzalik, R., and Winiarski, A. (2008) Lakargiite $CaZrO_3$: A new mineral of the perovskite group from the North Caucasus, Kabardino-Balkaria, Russia. American Mineralogist, 93, 1903–1910.

Galuskin, E.V., Gazeev, V.M., Lazic, B., Armbruster, T., Galuskina, I.O., Zadov, A.E., Pertsev, N.N., Wrzalik, R., Dzierzanowski, P., Gurbanov, A.G., and Bzowska, G. (2009) Chegemite $Ca_7(SiO_4)_3(OH)_2$—A new humite-group calcium mineral from the Northern Caucasus, Kabardino-Balkaria, Russia. European Journal of Mineralogy, 21, 1045–1059.

Galuskina, I.O., Galuskin, E.V., Dzierżanowski, P., Armbruster, T., and Kozanecki, M. (2005) A natural scandian garnet. American Mineralogist, 90, 1688–1692.

Galuskina, I.O., Lazic, B., Armbruster, T., Galuskin, E.V., Gazeev, V.M., Zadov, A.E., Pertsev, N.N., Jeżak, E., Wrzalik, R., and Gurbanov A.G. (2009) Kumtyubeite $Ca_5(SiO_4)_2F_2$—a new calcium mineral of the humite group from Northern Caucasus, Kabardino-Balkaria, Russia. American Mineralogist, 94, 1361–1370.

Galuskina, I.O., Galuskin, E.V., Armbruster, T., Lazic, B., Kusz, J., Dzierżanowski, P., Gazeev, V.M., Pertsev, N.N., Prusik, K., Zadov, A.E., Winiarski, A., Wrzalik, R., and Gurbanov, A.E. (2010a) Elbrusite-(Zr)—a new uranian garnet from the Upper Chegem caldera, Kabardino-Balkaria, Northern Caucasus, Russia. American Mineralogist, 95, in press.

Galuskina, I.O., Galuskin, E.V., Dzierżanowski, P., Gazeev, V.M., Prusik, K., Pertsev, N.N., Winiarski, A., Zadov, A.E., and Wrzalik, R. (2010b) Toturite $Ca_3Sn_2Fe_2SiO_{12}$—A new mineral species of the garnet group. American Mineralogist, 95, in press.

Gazeev, V.M., Zadov, A.E., Gurbanov, A.G., Pertsev, N.N., Mokhov, A.V., and Dokuchaev, A.Ya. (2006) Rare minerals of Verkhniy Chegem caldera (in skarned carbonates xenoliths in ignimbrites). Vestnik Vladikavkazskogo Nauchnogo Centra, 6, 18–27 (in Russian).

Hatert, F. and Burke, E.A.J. (2008) The IMA–CNMNC dominant-constituent rule revisited and extended. Canadian Mineralogist, 46, 717–728.

Kolesov, B.A. and Geiger, C.A. (1998) Raman spectra of silicate garnets. Physics and Chemistry of Minerals, 25, 142–151.

Kraus, W. and Nolze, G. (1996) POWDER CELL—a program for the representation and manipulation of crystal structures and calculation of resulting X-ray powder patterns. Journal of Applied Crystallography, 29, 301–303.

Levinson, A.A. (1966) A system of nomenclature for rare earth minerals. American Mineralogist, 51, 152–158.

Mandarino, J.A. and Back, M.E. (2004) Fleischer's Glossary of Mineral Species 2004, 309 p. Mineralogical Record Inc., Tucson.

Pasero, M., Kampf, A.R., Ferraris, C., Pekov, I.V., Rakovan, J., and White, T.J. (2010) Nomenclature of the apatite supergroup minerals. European Journal of Mineralogy, 22, 163–179, DOI: 10.1127/0935-1221/2010/0022-2022.

Rulmont, A., Tarte, P., Van Moer, A., Cartié, B., and Choisnet, J. (1995) Simultaneous occurrence of Sn^{4+} on the three cationic sites of the garnet structure: the solid solutions $Ca_xSn_xGa_{8-2x}O_{12}$ ($2.5 < x < 3.0$). Journal of Solid State Chemistry, 118, 6–9.

Schingaro, E., Scordari, F., Capitano, F., Parodi, G., Smith, D.S., and Mottana, A. (2001) Crystal chemistry of kimzeyite from Anguillara, Mountains. Sabatini, Italy. European Journal of Mineralogy, 13, 749–759.

Shannon, R.D. (1976) Revised effective ionic radii and systematic studies of interatomic distances in halides and chalcogenides. Acta Crystallographica, A32, 751–767.

Whittle, K.R., Lumpkin, G.R., Berry, F.J., Oates, G., Smith, K.L., Yudintsev, S., and Zaluzec, N.J. (2007) The structure and ordering of zirconium and hafnium containing garnets studied by electron channeling, neutron diffraction, and Mössbauer spectroscopy. Journal of Solid State Chemistry, 180, 785–791.

Zadov, A.E., Gazeev, V.M., Pertsev, N.N., Gurbanov, A.G., Yamnova, N.A., Gobechiya, E.R., and Chukanov, N.V. (2008) Discovery and investigation of a natural analog of calcio-olivine (γ-Ca_2SiO_4). Doklady of Earth Sciences RAS, 9, 1431–434 (in Russian).

Manuscript received November 8, 2009
Manuscript accepted February 21, 2010
Manuscript handled by Ian Swainson